CR-54525

apd

GD/A-BTD64-137

REPORT NO. 137

DATE 21 Aug. 1964

NO. OF PAGES 38

10-13

GENERAL DYNAMICS | ASTRONAUTICS

CENTAUR 1/10th Scale Model

Base Heating Study

NAS3-3232

PREPARED BY R. F. Yurczyk
R. F. Yurczyk

CHECKED BY E. D. Berlin
E. D. Berlin

APPROVED BY G. C. Wilson
G. C. Wilson
Thermo. Group Engr.

APPROVED BY R. S. Wentink
R. S. Wentink
Asst. Group Engr.
Design Analysis

REVISIONS

NO.	DATE	BY	CHANGE	PAGES AFFECTED

A 709-1 (REV. 1-62)

FOREWORD

An analysis of the results of a 1/10th-scale model base heating study, as applied to the full scale Centaur vehicle is presented. The test program was conducted by Cornell Aeronautical Laboratory, Inc., under contract with NASA Lewis Research Center. The test techniques and much of the support equipment used in this study were developed previously for base heating studies of the Saturn space launch vehicle.

Although base heating on a twin engine configuration such as Centaur is not as severe as on a clustered engine configuration, it was felt that a heating problem may exist. Therefore, the scale model base heating test program was initiated. The Centaur test program was initially set up to be dovetailed into the Saturn program on a non-interference basis. Later when the Centaur program was transferred to NASA, Lewis Research Center, the tests were conducted independently of the Saturn program.

TABLE OF CONTENTS

LIST OF ILLUSTRATIONS

SUMMARY

The 1/10th-scale model Centaur base heating program was conducted at Cornell Aeronautical Laboratory, (CAL) to determine the heating effects of the reverse flow field on components in the base region. The reverse flow is due to main engine exhaust jet interference at high altitude. Also, the reverse flow gas expands to temperatures below the freezing point of water so that ice particles could cause "sand blasting" of components in the base region. The results of the base heating program were used to determine if adequate insulation is provided on the temperature sensitive components in the base region.

The tests were conducted in a high altitude chamber using short duration testing techniques. A 1/10th-scale model simulating the aft portion of the Centaur vehicle from station 412 rearward was used. The scope of the program was to study the convective heating rates in the reverse flow field, to attempt to measure ice particle formation in the reverse flow field, and to determine scaling parameters to be used in applying the measured heat rates to the full-scale vehicle.

The heat flux survey tests were made at a simulated altitude of 360,000 feet. The data from one run at 450,000 feet was used to determine the heat flux variation with altitude.

Since the size of the scale model has some effect on the reverse flow field due to variation in Reynolds number with model size, the Reynolds number was varied by changing the chamber pressure.

The instrumentation used in the survey of the heat flux in the reverse flow field was mounted on rods of different sizes to provide scaling

information in applying the test data to the full scale components. Extrapolation of the scale model data is possible by correlation on the basis of the flow regime obtained for the attained test conditions.

The results of the tests, where chamber pressure was varied, along with information from Reference 4, indicated that scaling effects on the reverse flow field were small. Although scaling effects would cause a reduction in the measured heat flux, the actual flux would be reduced by cooling effects of the LOX boost pump turbine exhaust which was not included in the test. Also, the results of the test at 450,000 feet, the altitude at which Centaur main engine start occurs, shows that the measured rates at 360,000 feet are high by a factor of 1.25. Therefore, the measured heat flux can be applied directly to the full scale vehicle although they may be slightly conservative.

The results of the tests show that the reverse flow field is in the slip flow regime and approaches the free molecular regime at the base. Heat flux to components in this region would range from a maximum of 0.6 Btu/ft^2-sec nearest the nozzle exit to less than 0.2 Btu/ft^2sec at the base. The maximum heat rate at the base occurs on the X-axis approximately 21 inches from the center. The heat flux drops off rapidly from this point.

INTRODUCTION

The 1/10th-scale model Centaur base heating program was initiated to determine if the various components in the vehicle base region would be subject to over heating. It was felt that reverse flow in the base region due to main engine jet interference, in addition to radiation effects, might cause overheating of some of the temperature-sensitive components. Also, since the jet exhaust, which consists primarily of water vapor, will expand to temperatures below the freezing point of water, ice particles could be formed in the flow field. These particles would be accelerated toward the base of the vehicle by the reverse flow and, if they grow to sufficient size, will cause erosion and heating upon impact.

The study was conducted by Cornell Aeronautical Laboratory, using a short duration test technique developed by the laboratory for base heating studies of the clustered configuration for the Saturn space launch vehicle.

The scope of the 1/10th-scale model program was 1) to study the convective heating rates to the Centaur aft bulkhead and to various components mounted in the aft region; 2) to attempt to measure ice particle formation in the reverse flow field; and 3) to determine scaling parameters to be used in applying the measured heat rates to the full-scale vehicle.

During the planning stages of the base heating study program, consideration was being given to changing the Atlas-Centaur separation plane to a station aft of the 412 ring, leaving an extended skirt on

the Centaur vehicle. This extended skirt configuration would probably increase the heat transfer rate to the base by increasing the base pressure and was thus considered in the 1/10th-scale program. However, new separation techniques eliminated the lower separation plane requirement. Therefore, this portion of the base heating test program was deleted.

The proposed ice particle formation study would not have been a positive test because there was some doubt as to the feasibility of the testing techniques used. Ice particle formation in the model tests may have been effected by model dimensions. That is, the condensation kinetics may be dependent upon distance of travel between the nozzle exit plane and the base. Also, the temperature effects of the altitude chamber environment may effect ice particle growth.

The ice particle formation study portion of the program was deleted due to lack of funding, but a feasibility study of detecting ice particles in the reverse flow field using a light scattering technique was later carried out by Cornell Aeronautical Laboratory, using the Centaur 1/10th-scale model. No information pertaining to Centaur was obtained from this program.

DISCUSSION

Facility and Equipment: The 1/10th-scale model simulated the aft portion of Centaur from station 412 rearward. The model basically consisted of two unjacketed 40:1 expansion ration nozzles and the Centaur aft bulkhead with only the added equipment and protuberances which would have a major effect on the reverse flow field. The added equipment, which were removed for those tests requiring a clear base, were the helium storage bottles, the hydrogen peroxide bottles, and the boost pump sump. The engine nozzles were capble of being gimbaled 3 degrees in the yaw, pitch, or roll positions.

One component which may have a measurable influence on the heat transfer rate to the base but was not included in the model studies is the LOX boost pump turbine exhaust. This H_2O_2 exhaust system could not be simulated in these short duration tests without extensive development work which was beyond the scope of this program.

The combustor used to supply the 5 to 1 hydrogen-oxygen reaction products to the nozzles was a constant-pressure type developed by Cornell Aeronautical Laboratory (CAL) prior to the Centaur base heating study.

The tests were conducted in the 8 ft diameter, 25 ft long altitude chamber at CAL. The test facility and equipment are described in Reference 1.

INSTRUMENTA 'ION Thin film heat transfer gages developed at CAL and described in Reference 2 were used in measuring the heat flux to the base and to objects in the reverse flow field. Nine gages were

mounted on the base, as shown in Figure 1. Two of these at the center of the model were removed when the boost pump sump was mounted. Nine other gages were mounted on a movable rake which could be positioned in the region between the nozzles when the LOX sump and storage bottles were removed. The rake consisted of three pyrex rods of 1/8, 1/4 and 1/2 inch diameter sizes. Three thin film heat transfer gages were mounted on each rod. The rake could be moved parallel to or rotated about the model axis so that heat rates to the different diameter rods could be compared. The rake is shown in Figure 2.

These gages measure total heat flux, convective plus radiation heating. An attempt was made to measure the radiation heat flux using a quartz window placed over the film heat transfer gages. The window blocked out the convective heat but could allow radiation flux to reach the gage. However, quartz will transmit only a small percentage of total block body radiation in the low temperature range which comprises the major portion of the expanded exhaust plume. Therefore, although the gages indicated negligible radiation heat flux at the base, the actual flux may have been at a somewhat higher measurable value.

TEST RESULTS The different rod sizes were used to yield information from which heating rates to various wires, tubes, and other equipment in the base region could be determined, based on the base region flow configuration pertaining to the 1/10th-scale model. Extrapolation of this heating rate information to full-scale equipment dimensions is possible by correlating the scale model data on the basis of the flow regime obtained for the attained model test conditions. If the flow is continuous of a turbulent nature, the heat flux will scale as the -0.2 power of the diameter. For continuous laminar flow, the heat flux would scale as the -0.5 power of the diameter. For free molecular flow, there would be no rod diameter dependence.

However, complete knowledge of the dependence of base region flow on model scale factor was not provided by the test program. The main engine exhaust backflow may be influenced by engine exhaust gas viscosity effects, since the reverse flow consists of exhaust plume "fringe" gas which has been boundary layer flow within the nozzles. The nozzle boundary layer thickness is a function of the flow Reynolds number, which is proportional to model scale.

The nozzle stagnation pressure was varied in some of the tests to vary the Reynolds number and thus give an indication of the effect of the nozzle exit boundary layer on the reverse flow field. However, in varying the stagnation pressure, the jet exit pressure to ambient pressure ratio was also varied. This ratio may have a significant effect on jet plume interference, and thus on the reverse flow field. Therefore, caution must be exercised in interpreting these results.

The results of the variable chamber pressure runs are shown in Figure 3. These were run at a constant ambient pressure of 0.038 microns of mercury (0.038μ of Hg). From the average slope of these curves it can be seen that the heat transfer ratio varies approximately as the 1.5 power of the chamber pressure. Reference 3 shows that the total temperature, viscosity, and specific heat ratios remain approximately constant over this range of chamber pressure. Therefore, the Reynolds number is directly proportional to the chamber pressure or $\dot{q}$ (heat flux) is proportional to the 1.5 power of the nozzle flow Reynolds number. However, the base pressure and thus density of the reverse flow field will be effected by the variation in chamber pressure. Reference 4 shows results of base heating tests of the Saturn S-IV six engine configuration. Total pressure probes located outside the engine cluster between two adjacent engines indicated that the base

pressure varies almost directly as the chamber pressure even in tests with constant ambient pressure. This was especially true in the lower pressure regions of the base. Also, heat rate probes in the same location in these S-IV tests show that the heat transfer rate varied as the 1.4 power of the base pressure. Although the S-IV tests were run at a much higher ambient pressure than the Centaur tests, from these data it may be concluded that the heat transfer rate is affected by only a small factor due to scaling.

The rates measured in the Centaur 1/10th-scale test are conservative in that they were conducted at a lower simulated altitude than actual flight. The tests were conducted at a simulated altitude of 360,000 ft. (0.038 μ of Hg) whereas actual Centaur engine firing occurs at 450,000 ft. (0.006 μ of Hg). Figure 4 shows the heat flux variation with altitude. These tests were made with the rake 4.2 inches forward of the nozzle exit plane with the various heat transfer gages in the positions shown in Figures 3 and 4. It can be seen that the minimum slope, n in the expression $\dot{q} \propto P_A^{+n}$ is 0.065 with an average value of 0.12. The measurements from Q12 and Q15 (Figure 3) were ignored because they appeared to be erratic throughout the test program. Therefore, the test data at 360,000 ft. is an average factor of 1.25 times greater than the heat rate at 450,000 feet.

Reference 4 also shows that secondary exhaust flow into the base region decreases the maximum heat flux to 0.6 times the maximum flux of 2.9 Btu/ft^2-sec. with no secondary exhaust flow. This reduction in heat rate is probably due to blanketing of the base with the cooler secondary exhaust gases and will probably apply to the Centaur vehicle.

Therefore, it can be assumed that any scale factor affecting the heat transfer rate due to nozzle boundary layer scaling will be compensated for by the increased altitude and the turbine exhaust gas effect. Therefore, no scaling factor need by applied, other than that of equipment dimensions, as obtained from the rake data and explained in the following paragraphs.

All tests made to determine the heat flux profile at the base and in the reverse flow field were made with a chamber pressure of 300 psia and an ambient pressure of 0.038 μ of Hg.

The rake survey tests in the reverse flow field were made with the engines in a null gimbal position. The bulk of the tests were made to find the heat transfer rate variation with rod size and to find the change of heat rate along the axis of the model between the base and the nozzle exit plane. The heat transfer rates were measured at the center line of the model, at 3/4 inch from center on the Y-axis, at 1-3/8 inches from center on the X-axis, and at the X-Y coordinates (1-3/8", 3/4") on the model. Measurements were made at three different positions from the nozzle exit plane, as shown in Figure 2. Figures 5 through 8 show the measured heat rates at the various positions in the reverse flow field.

The heat flux to the 1/8-inch rod at the center line of the model (Figure 5) varies from 1.15 Btu/ft^2 sec at 3.6 inches from the nozzle exit plane to 0.65 Btu/ft^2 sec at 4.8 inches. The flux to the 1/2-inch rod was lower, varying from 0.8 to 0.6 Btu/ft^2 sec over the same range.

At 3/4 inch from center on the Y-axis, the heat flux to all three rods was almost constant over the range, 3.6 inches to 4.8 inches from the nozzle exit. This heat flux as shown in Figure 6, is approximately 0.4 Btu/ft^2 sec.

At 1-3/8 inches from center on the X-axis, the heat flux varied from 1.05 to 0.68 Btu/ft^2 sec to the 1/8-inch rod, and from 0.90 to 0.57 Btu/ft^2 sec to the 1/2-inch rod.

The scatter in the data, in particular the extremely low points shown in Figures 5 through 8, is due to electrical fault in the instrumentation. These points were neglected in the analysis of the data.

The heat transfer rates at the X-Y coordinates (1-3/8", 3/4") show more scatter than at the other positions on the rake. This can probably be credited to the fact that this position is in the high Mach number, low density region of the reverse flow field where the rates of change of velocity and density are very high. In this region, the flow approaches the free molecular regime where the heat transfer rate is proportional to ρV^2, where P is the density of the approaching gas stream and V is the velocity of approach. Since the heat flux is quite low in this region, small variations in the velocity of the flow field will cause much scatter in the data.

Figure 8 also shows that the heat transfer rate to the 1/4-inch rod is lower than the heat rate to the 1/2-inch rod at the (1-3/8, 3/4) coordinate. This contradicts the laws of heat transfer and is probably due to electrical bias in one or more of the heat flux gages. These data were not included in determining the scale factors from variation of heat rate with rod diameter.

Reference 5 shows that the film heat transfer coefficients for cylinders in the continuous flow regime are approximately:

$$h \propto \frac{\rho V}{D^{0.2}} \quad \text{(turbulent)}$$

$$h \propto \frac{\rho V}{D^{0.5}} \quad \text{(laminar)}$$

In the free-molecular regime, the heat transfer rate is independent of rod diameter.

The mean free path of the engine exhaust products, λ_m, is about 10^{-5} cm at a pressure of one atmosphere. Since λ_m is inversely proportional to pressure, if the reverse flow field is expanded to ambient pressure, the mean free path is:

$$\lambda_m = (P_o/P_{amb})\lambda_{m_o} = 200 \text{ cm}$$

The rod diameters are in the order of 1 cm. Therefore, the Knudsen number which is defined as λ_m/D is approximately 200 for the conditions stated above. Reference 6 shows that the free molecular flow regime exists for Knudsen numbers greater than 1.0. Therefore, the reverse flow could be in the free molecular regime at the point where the rods are encountered.

In Figure 10, the slope, n, from the expression

$$\dot{q} \propto (D)^{-n} \qquad (1)$$

is shown to vary from 0.27 to 0.05 at the center of the model, where q is the heat flux in Btu/ft^2 sec and D is the rod diameter. Writing:

$$N_u \propto (R_e)^m \tag{2}$$

where N_u is the Nusseld number and Re is Reynolds number. The result is

$$\frac{hD}{k} \propto \left(\frac{\rho VD}{\mu}\right)^m \tag{3}$$

where

- h = film heat transfer coefficient
- D = rod diameter
- k = thermal conductivity of the rod
- ρ = gas density
- μ = gas viscosity

The heat flux can be written as:

$$\dot{q} = h \Delta T \text{ or } \dot{q} \propto h \tag{4}$$

Then, from equation (1)

$$h \propto (D)^{-n} \tag{5}$$

and from equation (3)

$$n = 1 - m \tag{6}$$

Therefore, at the center line of the model, at Station 3, $N_u \propto R_e^{0.73}$ and at Station 1, N_u $R_e^{0.95}$. At 3/4 inches from center on the Y-axis m varies from 0.775 to 0.815. At 1-3/8 inches from center on the X-axis m is nearly constant at 0.89.

Reference 7 shows that with values of m in this range, the reverse flow is probably in the slip regime between continuum laminar and free molecular. For slip flow, the Knudsen number is approximately 0.1, so the estimated pressure at the center line in the reverse flow field is near 100 microns of Hg at Station 3 and approaches 10 microns of Hg at the base.

The equipment mounted in the base region of Centaur is located forward of Station 1. Therefore, $m \geq 0.8$ would apply in scaling the heat flux to various size wires and equipment on Centaur.

To get a more complete profile of the heat flux in the reverse flow field, the rake was rotated 90° from the position where the above data were measured. The gage locations for the rake in both positions is shown in Figure 11. Tests were run at each of the three stations shown in Figure 2 with the rake in the 90° position. By interpolation of all the rake data, the heat flux distribution at each of the three stations was estimated as shown in Figures 12 through 14. Also, the heat flux profile at Station 1 is shown in Figure 15.

The heat flux to the base was measured with the engines in a null gimbal position, as well as 3 degrees in yaw, pitch and roll. In one test with no gimballing, the base was cleared of the LOX sump and storage spheres. In all other base heat flux tests this extra equipment was included. The results of the tests are shown in Figures 16 and 17. The points shown to the left of center in Figure 16 were interpolated from the values measured 30 degrees on each side of the axis.

Although no repeat runs were made with any of these gimbal configurations, the data are felt to be valid because it follows the expected trends. The heat flux is low at the center where the gas density is high, but the velocity is very low. Expanding from the center, the product ρV increases, reaches a peak at about 2.2 inches from the model center, and then decreases as ρ rapidly decreases.

Figure 17 shows that the heat flux is highest along the X-axis, the jet interference line, and decreases rapidly on either side. The various engine gimbal runs showed increased heat flux to the base over the null gimbal cases. Although it can not be readily explained, the yaw gimbal position gave highest heat flux values reaching a maximum of 0.19 Btu/ft^2 sec 10° from the X-axis. These data were higher by a factor of 2 than the data from the other run. These high measured rates may be due to instrumentation error, but no proof is available. Therefore, it will be assumed that these rates are correct and can be expected on the full scale vehicle.

CONCLUSIONS AND RECOMMENDATIONS The reverse flow field is in the slip flow regime at points near the nozzle exit plane and approaches the free molecular regime near the aft bulkhead. The highest convective heat flux in the base region of the Centaur vehicle occurs along the X-axis. The heating rate is sharply reduced at points on either side of this axis. Also, the heating rate decreases with the changing flow regime with distance from the nozzle exit plane.

Because of this variation of heat flux with position in the base region, each temperature sensitive component must be analyzed separately to determine if it is adequately protected from engine plume heating.

The heat flux to small components mounted on the aft bulkhead will be comparable to that of the aft heat shield at similar surface temperatures. Tubes, wire bundles and any other small components aft of the base, near the X-axis of the vehicle will be subject to higher heat flux than the heat shield since the flow field in these regions is in the slip-flow regime.

The convective heat flux values measured in the 1/10th-scale model tests are directly applicable to components in the aft region of the vehicle. These values are slightly conservative, because they were measured at an altitude below which the Centaur stage operates. Also, the LOX boost pump turbine exhaust, which may have some cooling effect at the base, was not included in the 1/10th-scale tests.

No radiation heat flux information was obtained from this test program. The radiant flux to components in the aft region has been estimated from 1/40th-scale tests and Atlas flight data. However, this was a crude estimate and may be in error.

Therefore, both total and convective heat transfer calorimeters should be installed on the Centaur R&D vehicles to provide data with which the CAL 1/10th-scale model test information may be correlated, as well as provide direct information, including radiation data relative to the actual flight environment.

REFERENCES

1. "Base Heating of a 1/10-Scale Model Centaur Stage Using Short Duration, High Altitude Testing Techniques", C. L. Mathis, CAL Report No. AA-1773-Y-1, July 1963

2. "The Application of Short-Duration Techniques to the Study of Base Heating", K. D. Bird, et al, CAL Report No. HM-1510-Y-1 (I), April 1962

3. "Theoretical Performance of LH2 with LO2 as a Rocket Propellant", S. Gordon and B. McBride, NASA Memo, 5-21-59E, June 1959

4. "High Altitude Base Heating and Pressure Distribution Investigations On The Saturn S-IV 6-Engine Rocket Using Short Duration Techniques", CAL Report No. HM-1510-Y-3, June 1963

5. "Heat Transfer", McAdams, McGraw-Hill Co., 1954

6. "Molecular Flow of Gases", G. Patterson, Wiley, 1956

7. "Heat Transfer from Transverse and Yawed Cylinders in Continuum, Slip and Free Molecular Air Flow", L. Baldwin et al, ASME Transactions, May 1960

CENTAUR BASE INSTRUMENTATION LAYOUT

Notes:

T_1 - T_9 are thin film temperature gages

T_8 and T_9 are only in place when LOX boost pump sump is removed

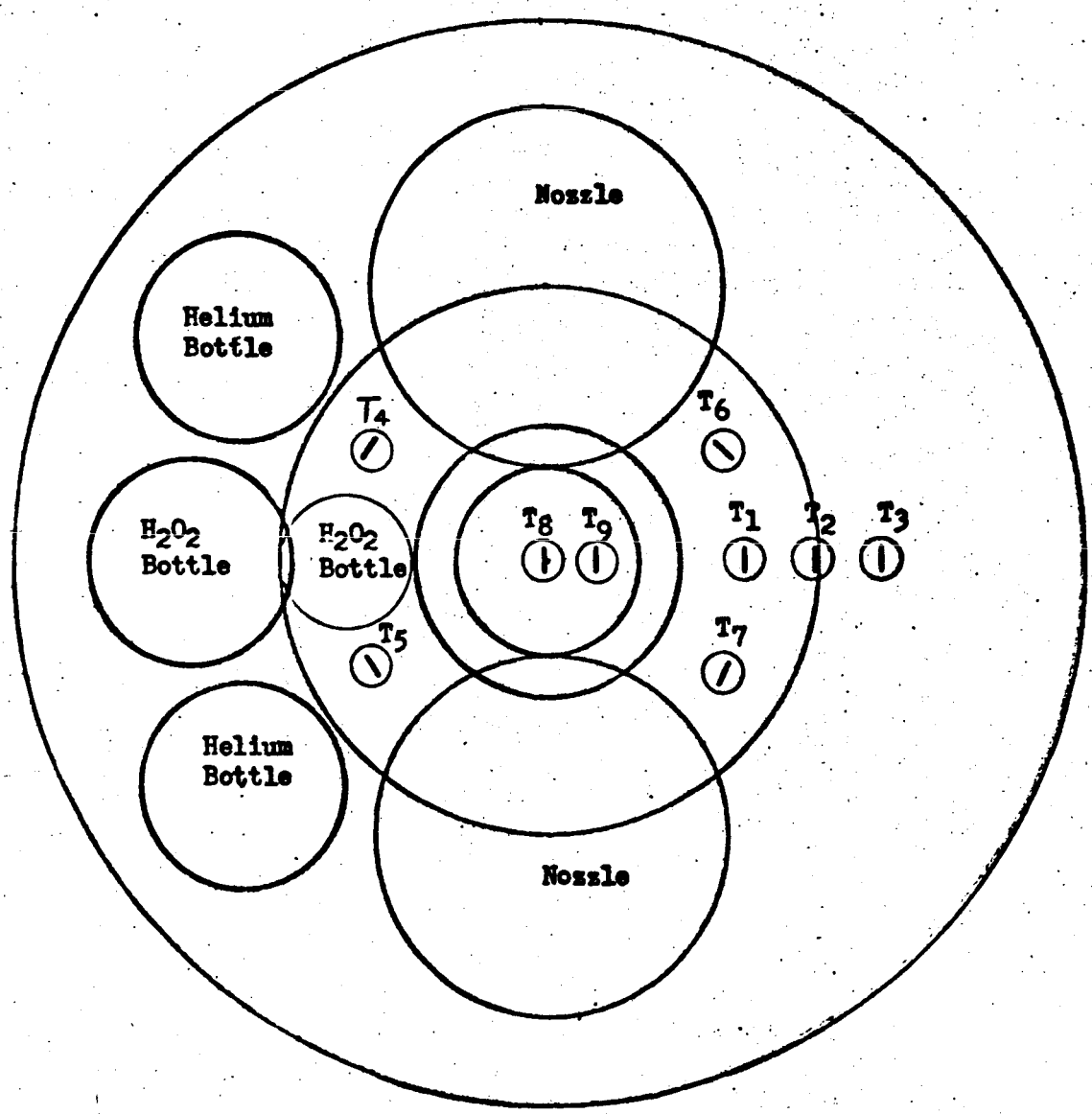

FIGURE 1

1/10th Scale Centaur Base Heating Model with Heat Transfer Rake

Station 1 - 4.8 inches from nozzle exit plane
Station 2 - 4.2 inches from nozzle exit plane
Station 3 - 3.6 inches from nozzle exit plane

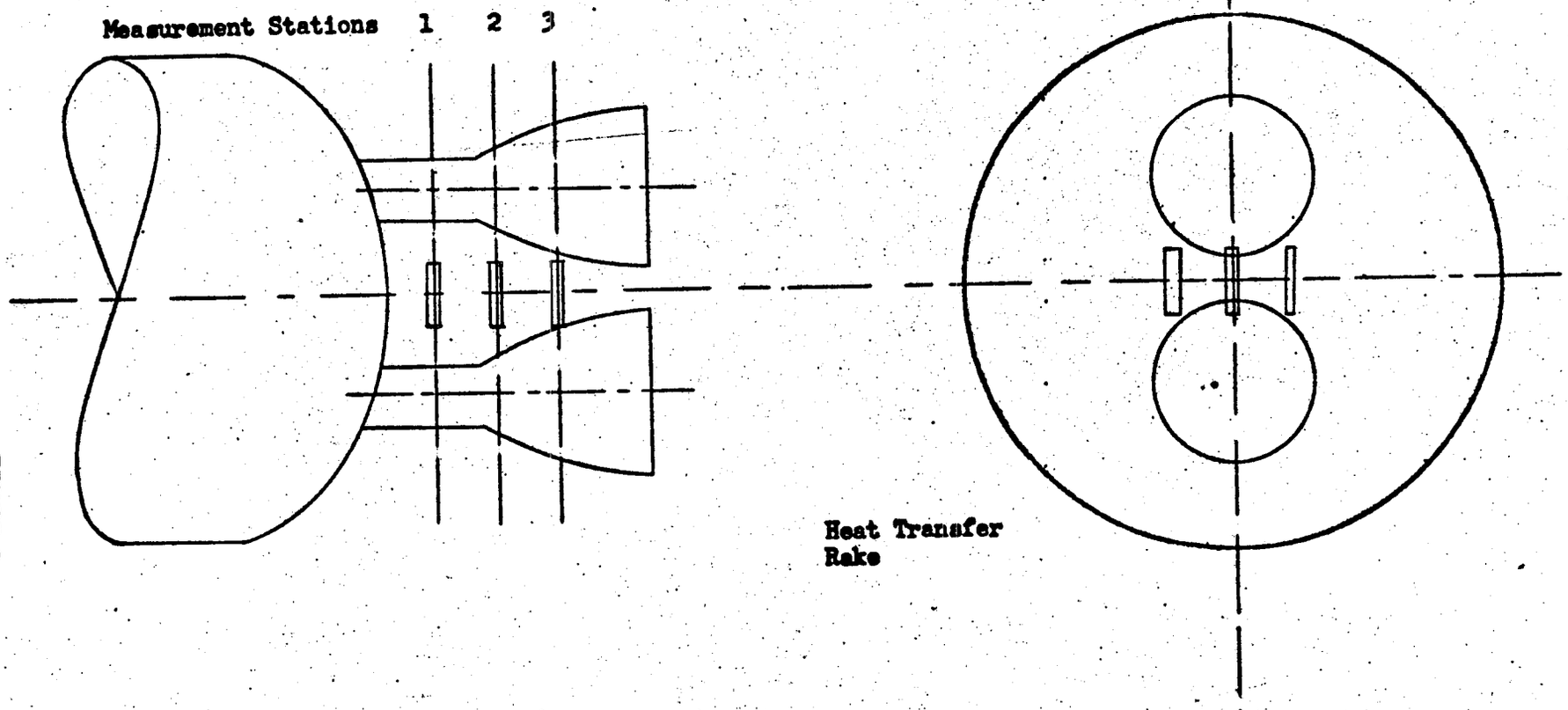

FIGURE 2

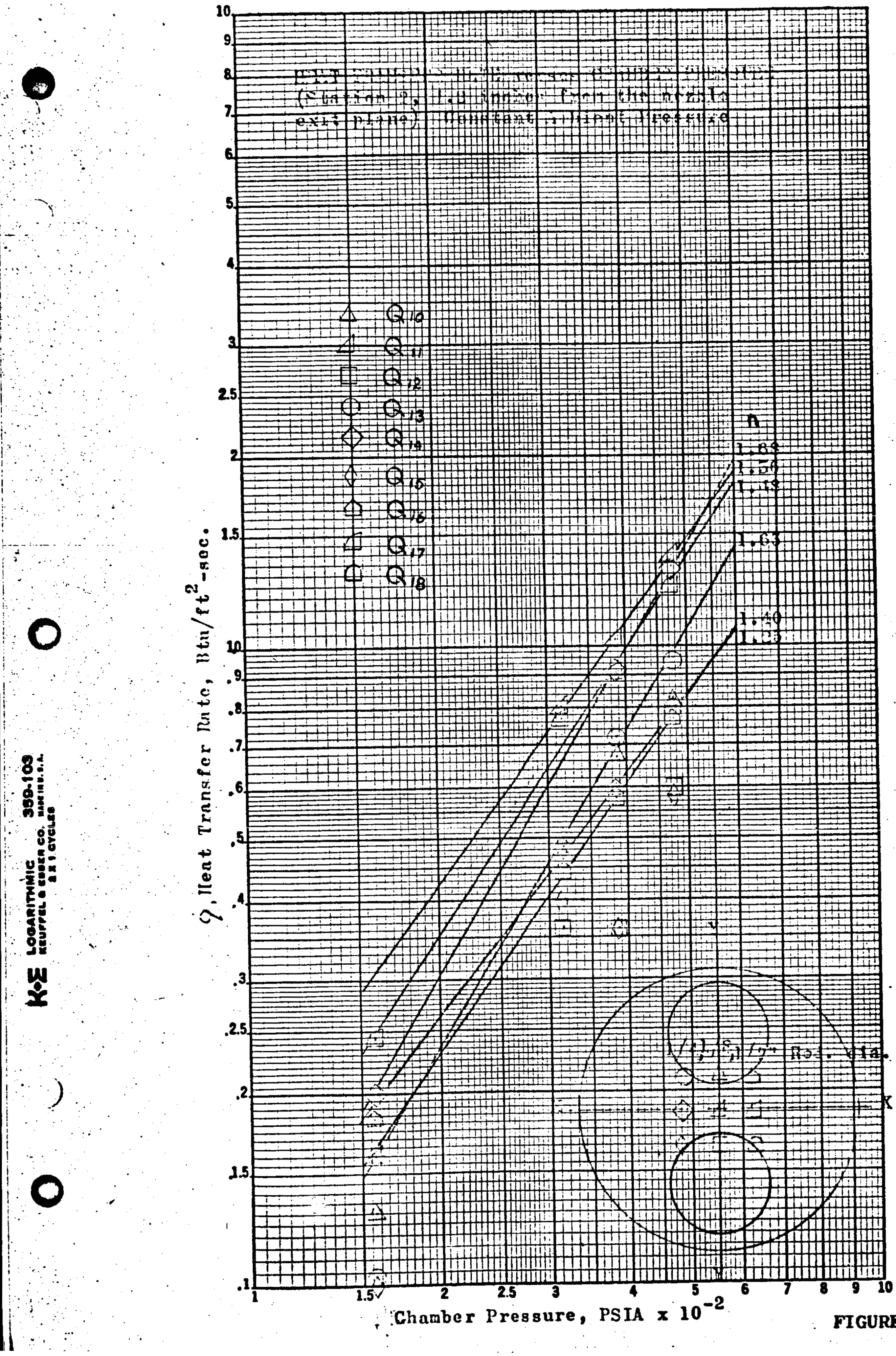
exit plane)
Q10
Q11
Q12
Q13
Q14
Q15
Q16
Q17
Q18
n
1.63
1.40
q, Heat Transfer Rate, Btu/ft2-sec.
Chamber Pressure, PSIA x 10-2
K&E LOGARITHMIC 359-103
KEUFFEL & ESSER CO.
2 X 1 CYCLES

FIGURE 3

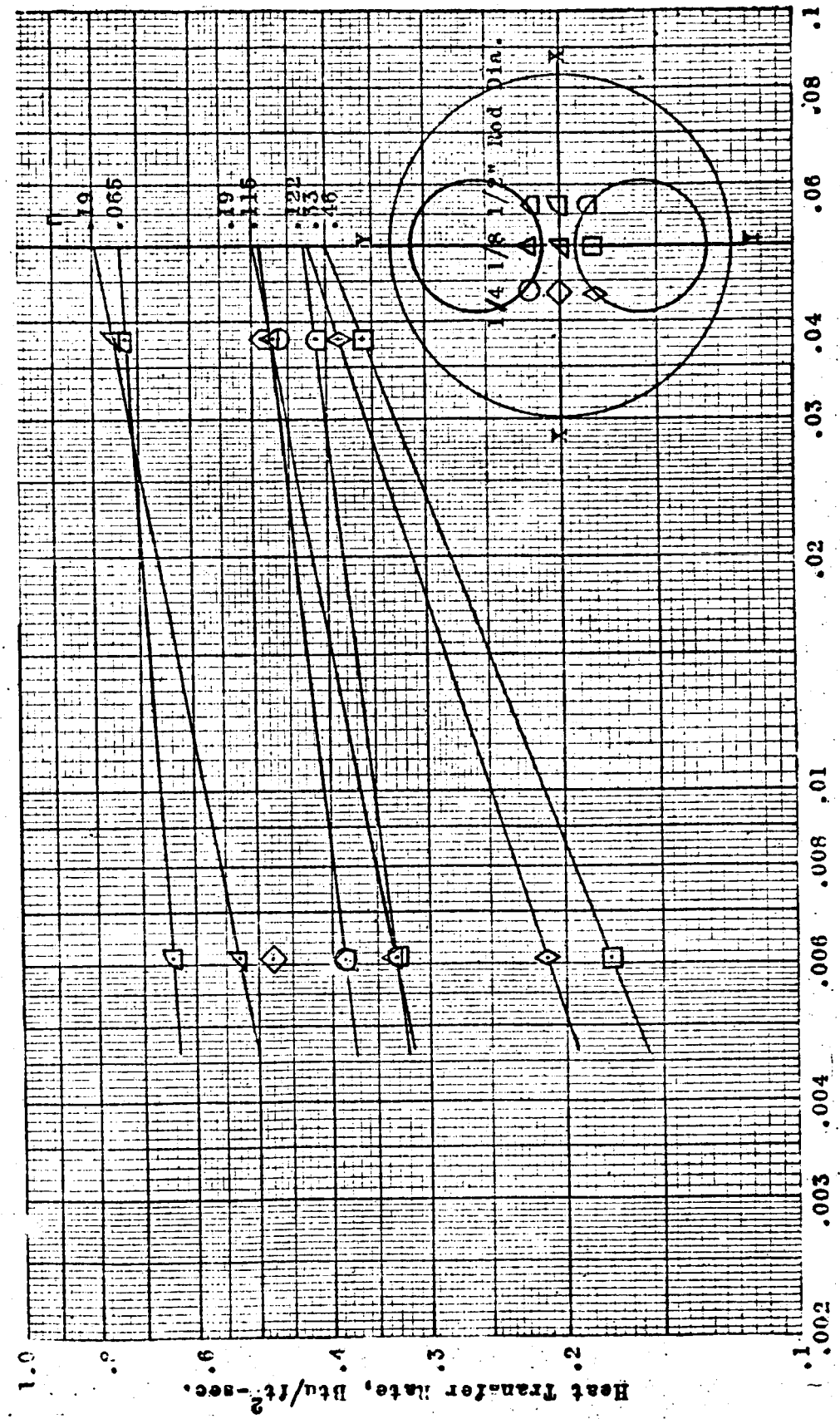

HEAT TRANSFER RATE versus AMBIENT PRESSURE AT
STATION 2, 4.2 inches from Nozzle Exit Plane

FIGURE 4

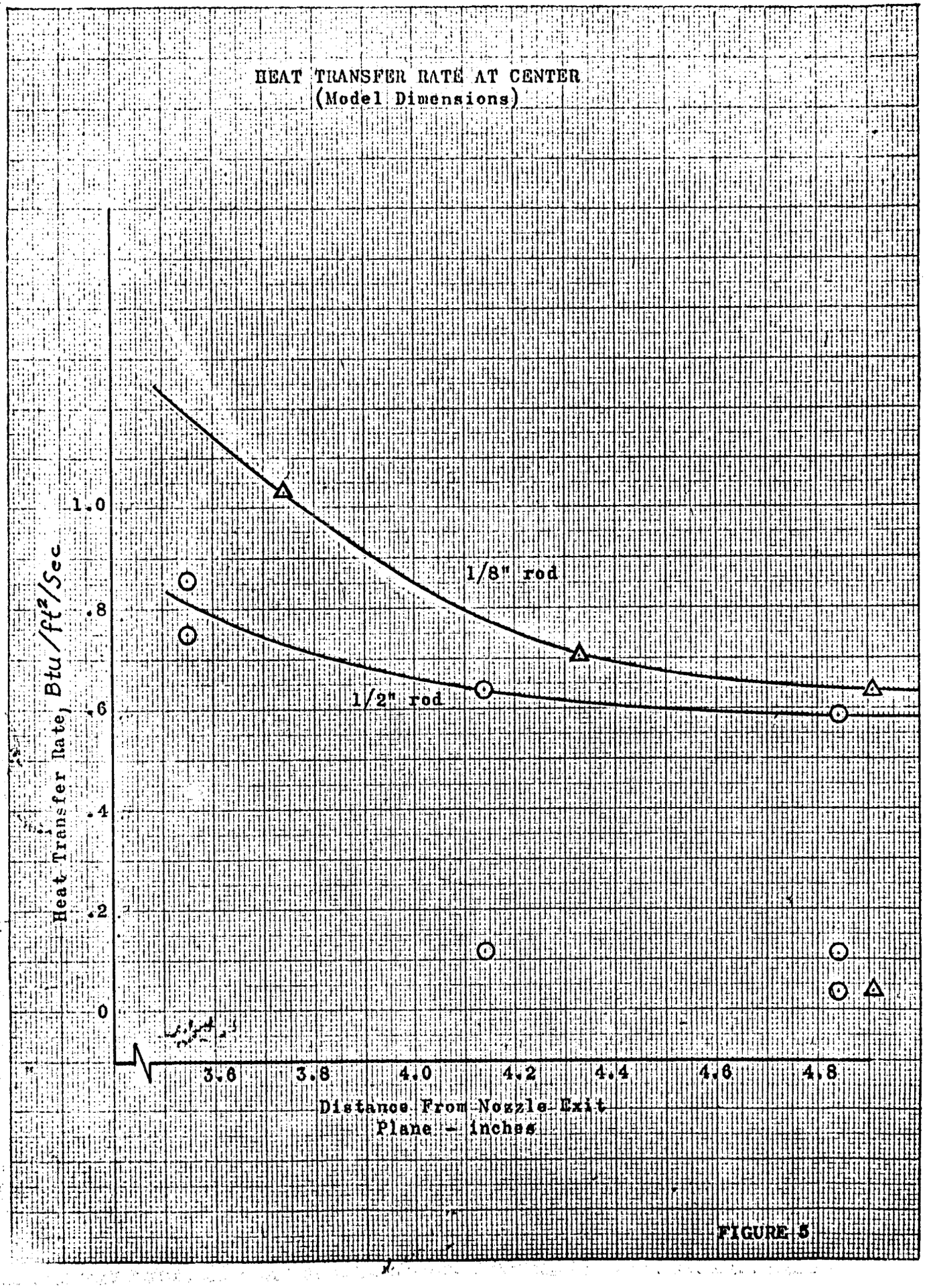
HEAT TRANSFER RATE AT CENTER
(Model Dimensions)
Heat Transfer Rate, Btu/ft²/Sec
1.0
.8
.6
.4
.2
0
1/8" rod
1/2" rod
3.6
3.8
4.0
4.2
4.4
4.6
4.8
Distance From Nozzle Exit
Plane - inches

FIGURE 5

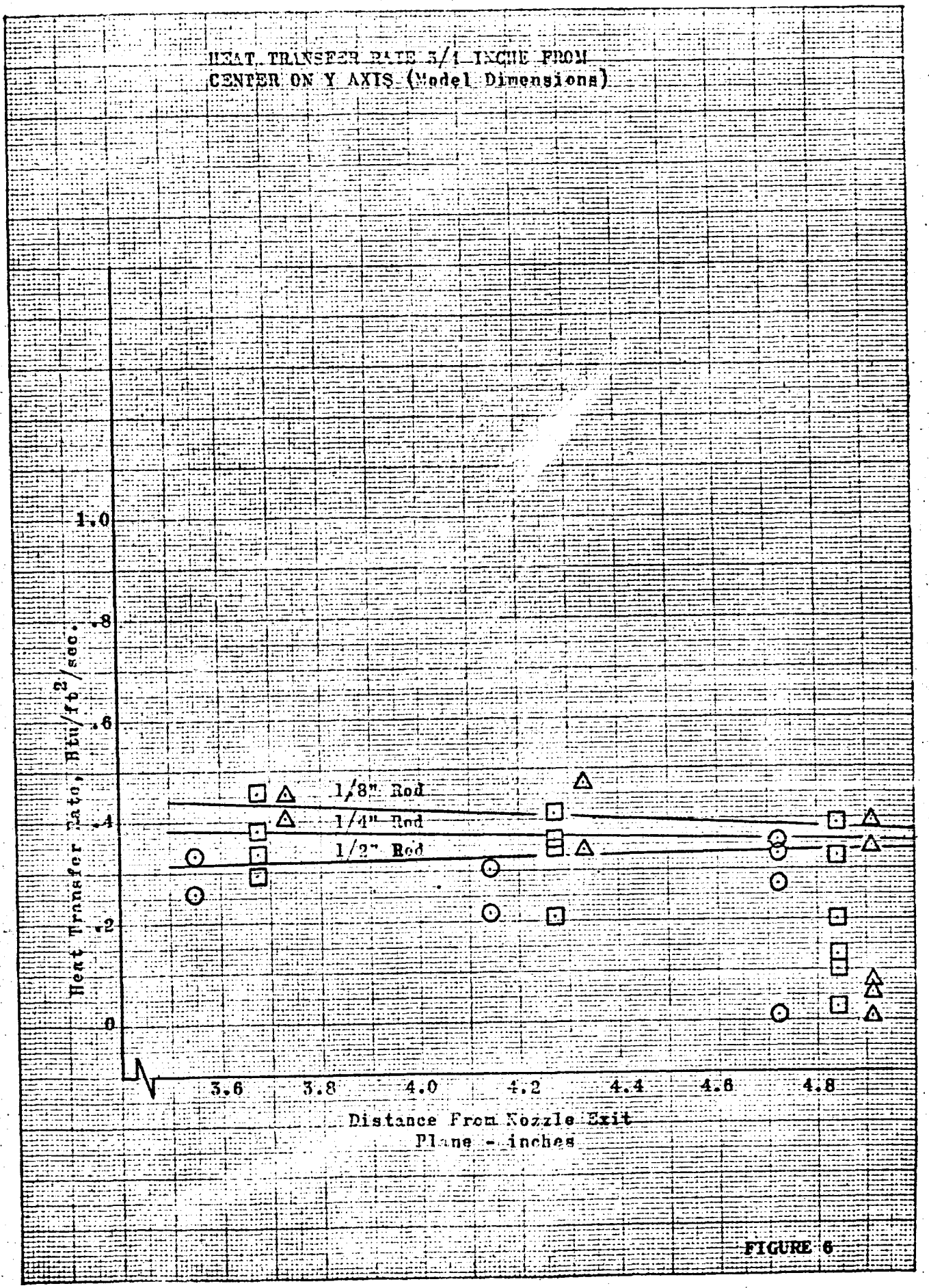
HEAT TRANSFER RATE 3/4 INCHE FROM
CENTER ON Y AXIS (Model Dimensions)
1.0
.8
.6
.4
.2
0
Heat Transfer Rate, Btu/ft²/sec.
1/8" Rod
1/4" Rod
1/2" Rod
3.6
3.8
4.0
4.2
4.4
4.6
4.8
Distance From Nozzle Exit
Plane - inches

FIGURE 6

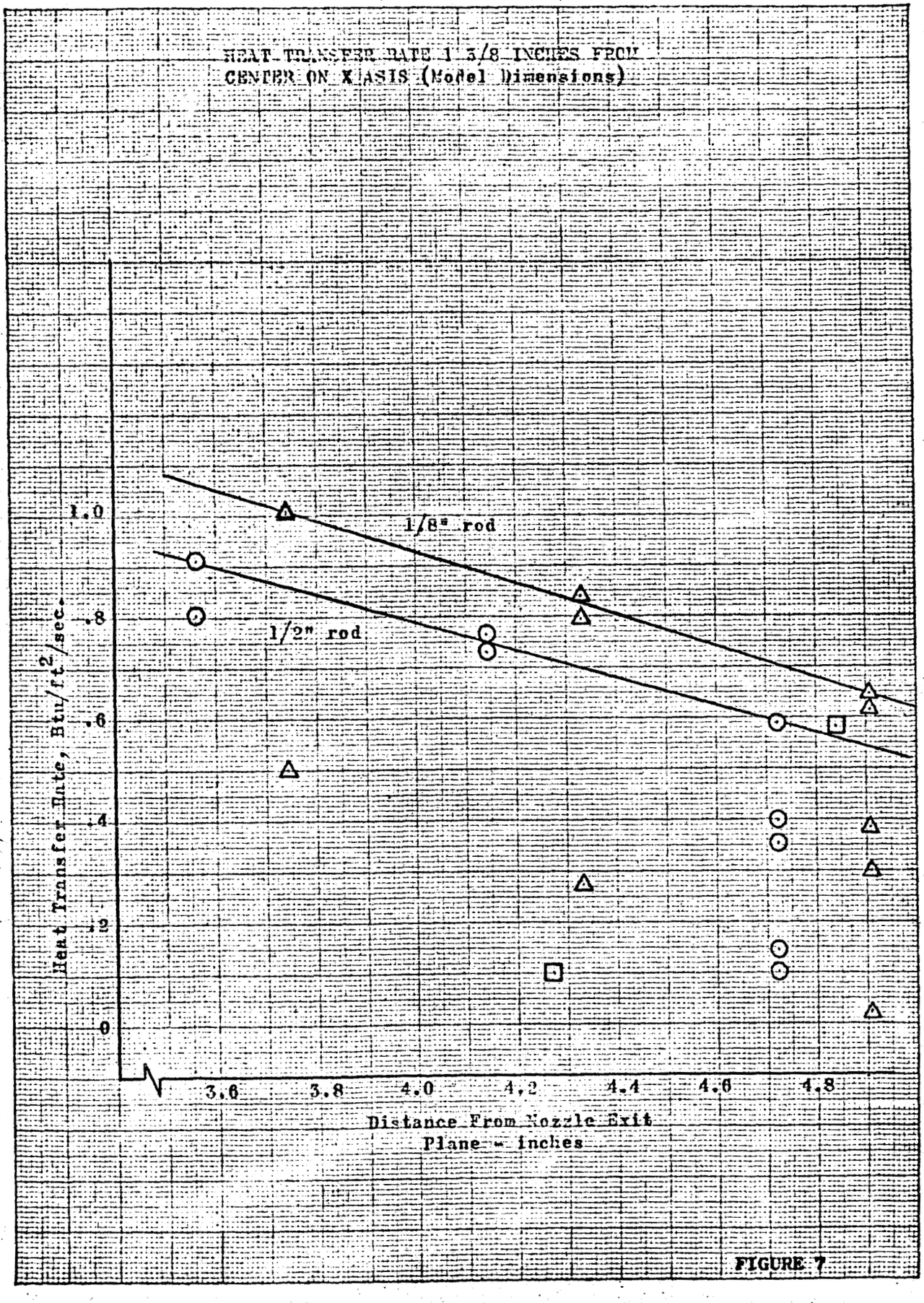
HEAT TRANSFER RATE 1 3/8 INCHES FROM
CENTER ON X AXIS (Model Dimensions)
1/8" rod
1/2" rod
Heat Transfer Rate, Btu/ft²/sec.
1.0
.8
.6
.4
.2
0
3.6
3.8
4.0
4.2
4.4
4.6
4.8
Distance From Nozzle Exit
Plane - Inches

FIGURE 7

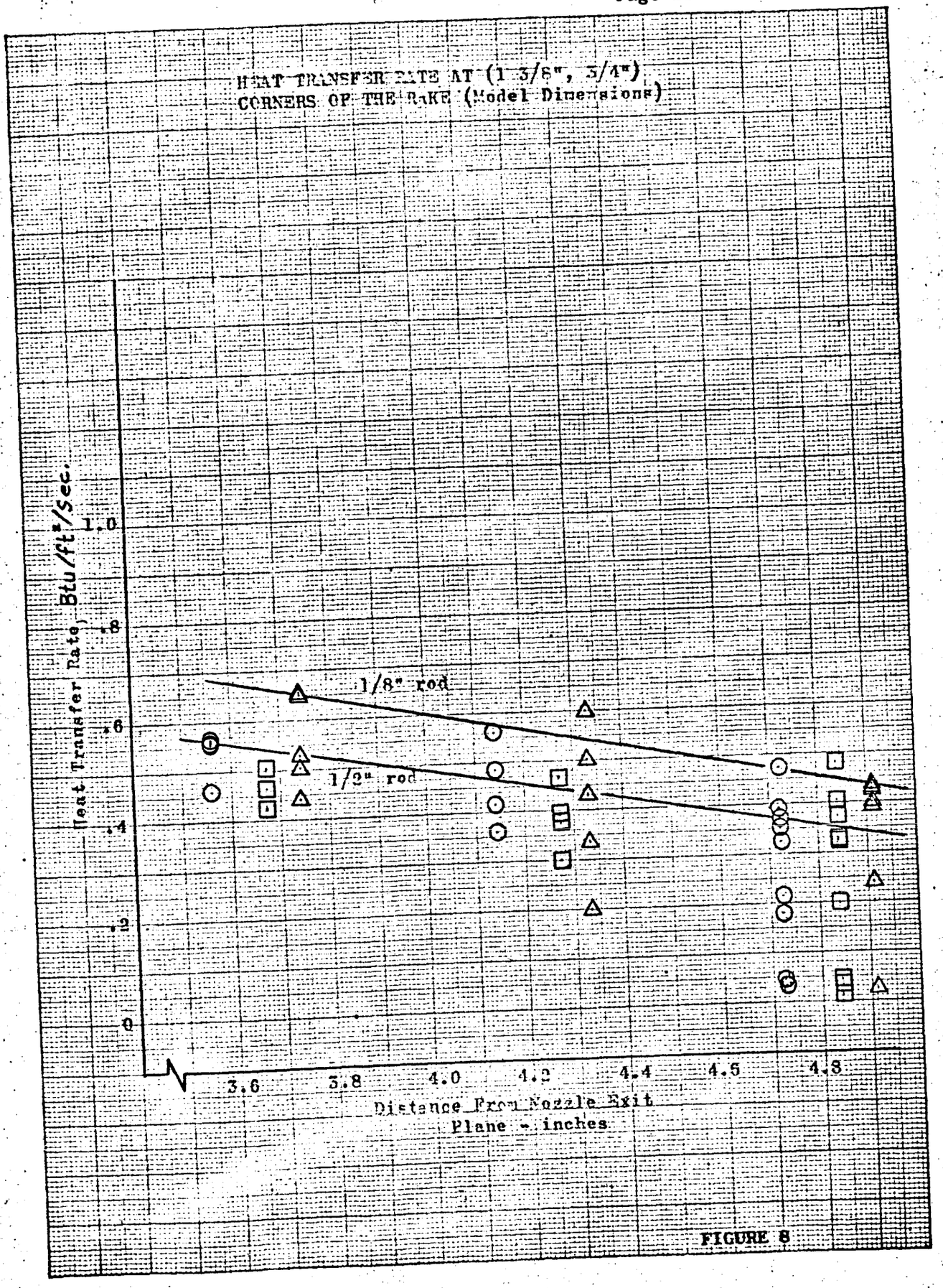
HEAT TRANSFER RATE AT (1 3/8", 3/4")
CORNERS OF THE RAKE (Model Dimensions)
Heat Transfer Rate, Btu/ft²/Sec.
1.0
.8
.6
.4
.2
0
1/8" rod
1/2" rod
3.6
3.8
4.0
4.2
4.4
4.6
4.8
Distance From Nozzle Exit Plane - inches

FIGURE 8

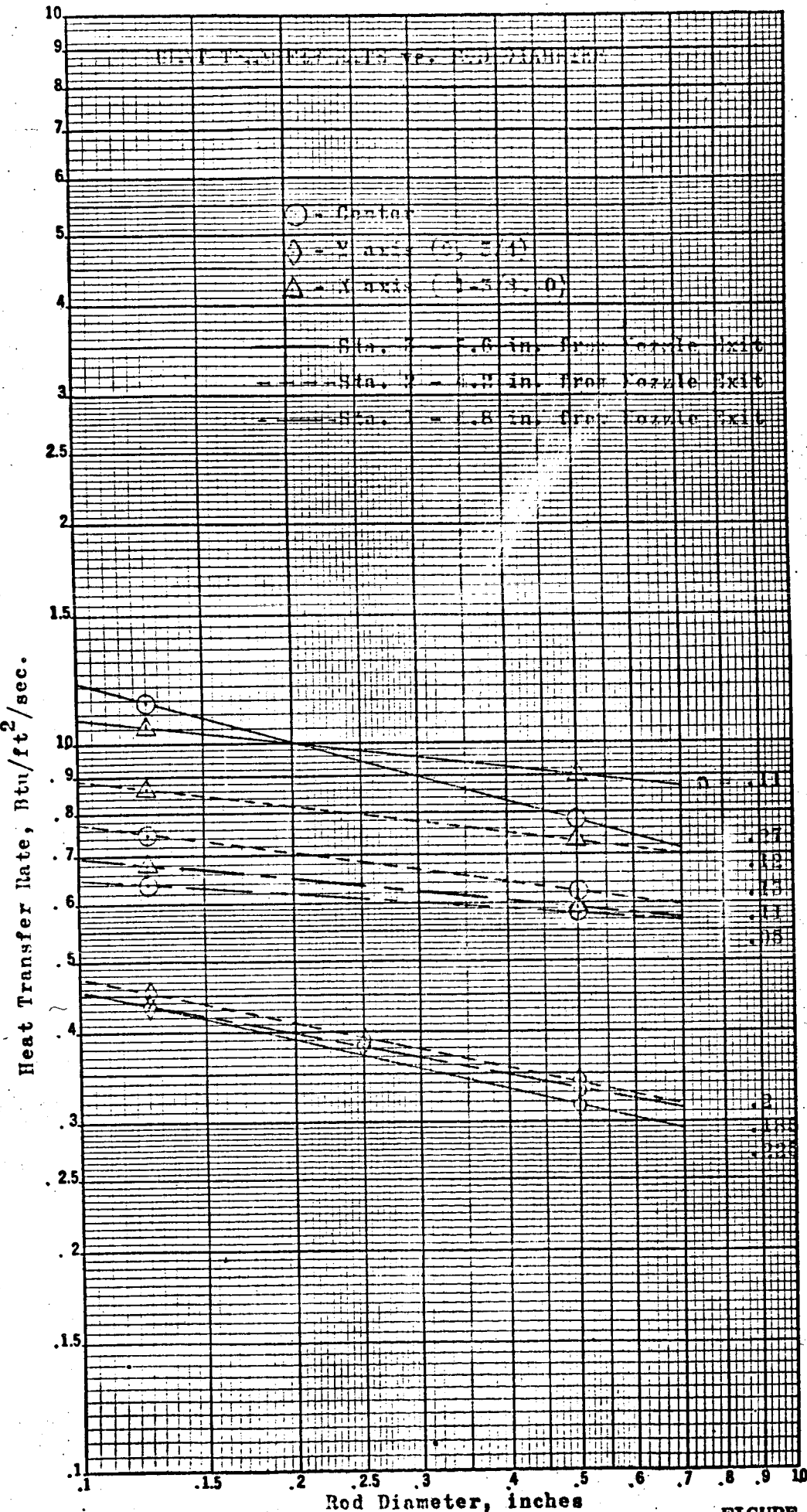
Heat Transfer Rate, Btu/ft²/sec.
Rod Diameter, inches
10
9
8
7
6
5
4
3
2.5
2
1.5
1
.9
.8
.7
.6
.5
.4
.3
.2
.1
.15
.25
.5
.6
.7
.8
.9
10
○ - Center
▷ - Y axis (0, 3.4)
△ - X axis (3.4, 0)
Sta. 7 - 5.6 in. from nozzle exit
Sta. 2 - 4.2 in. from nozzle exit
Sta. 1 - 1.8 in. from nozzle exit
P = .01
.07
.13
.15
.11
.05
.2
.1
.05

FIGURE 9

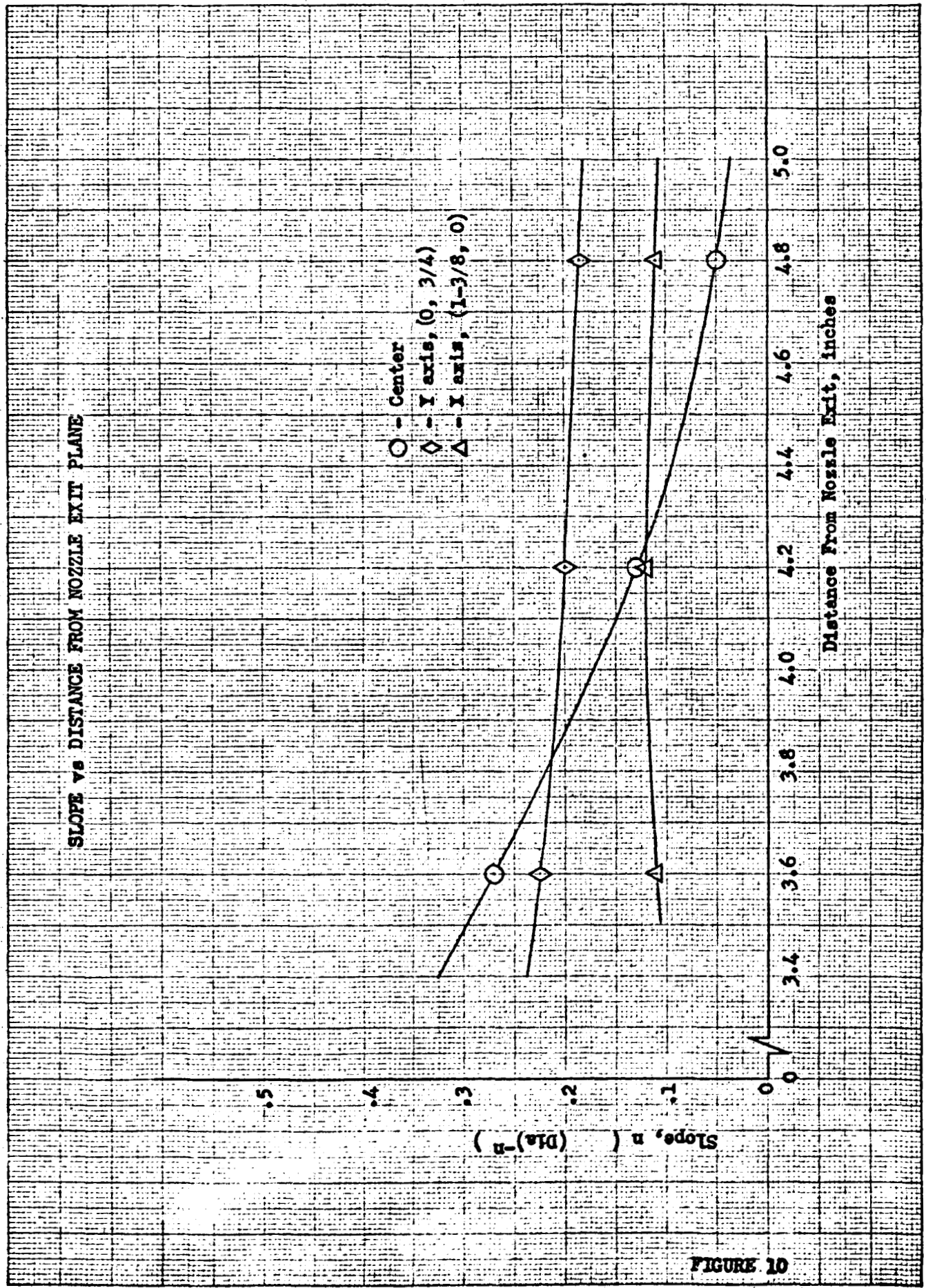
SLOPE vs DISTANCE FROM NOZZLE EXIT PLANE
○ - Center
◇ - Y axis, (0, 3/4)
△ - X axis, (1-3/8, 0)
Slope, n ((Dia)^-n)
Distance From Nozzle Exit, inches
0
.1
.2
.3
.4
.5
3.4
3.6
3.8
4.0
4.2
4.4
4.6
4.8
5.0

FIGURE 10

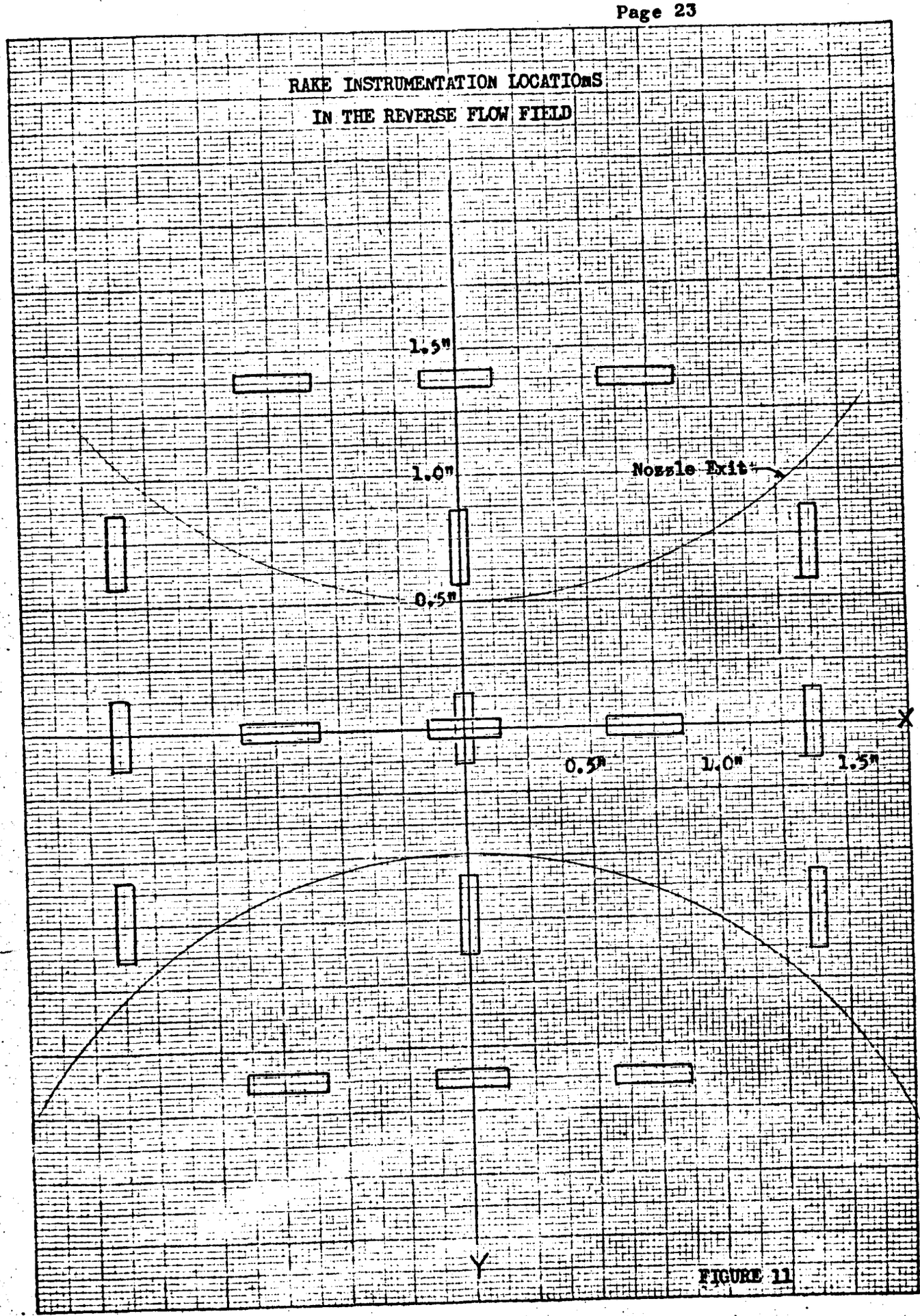
RAKE INSTRUMENTATION LOCATIONS
IN THE REVERSE FLOW FIELD
1.5"
1.0"
Nozzle Exit
0.5"
X
0.5"
1.0"
1.5"
Y

FIGURE 11

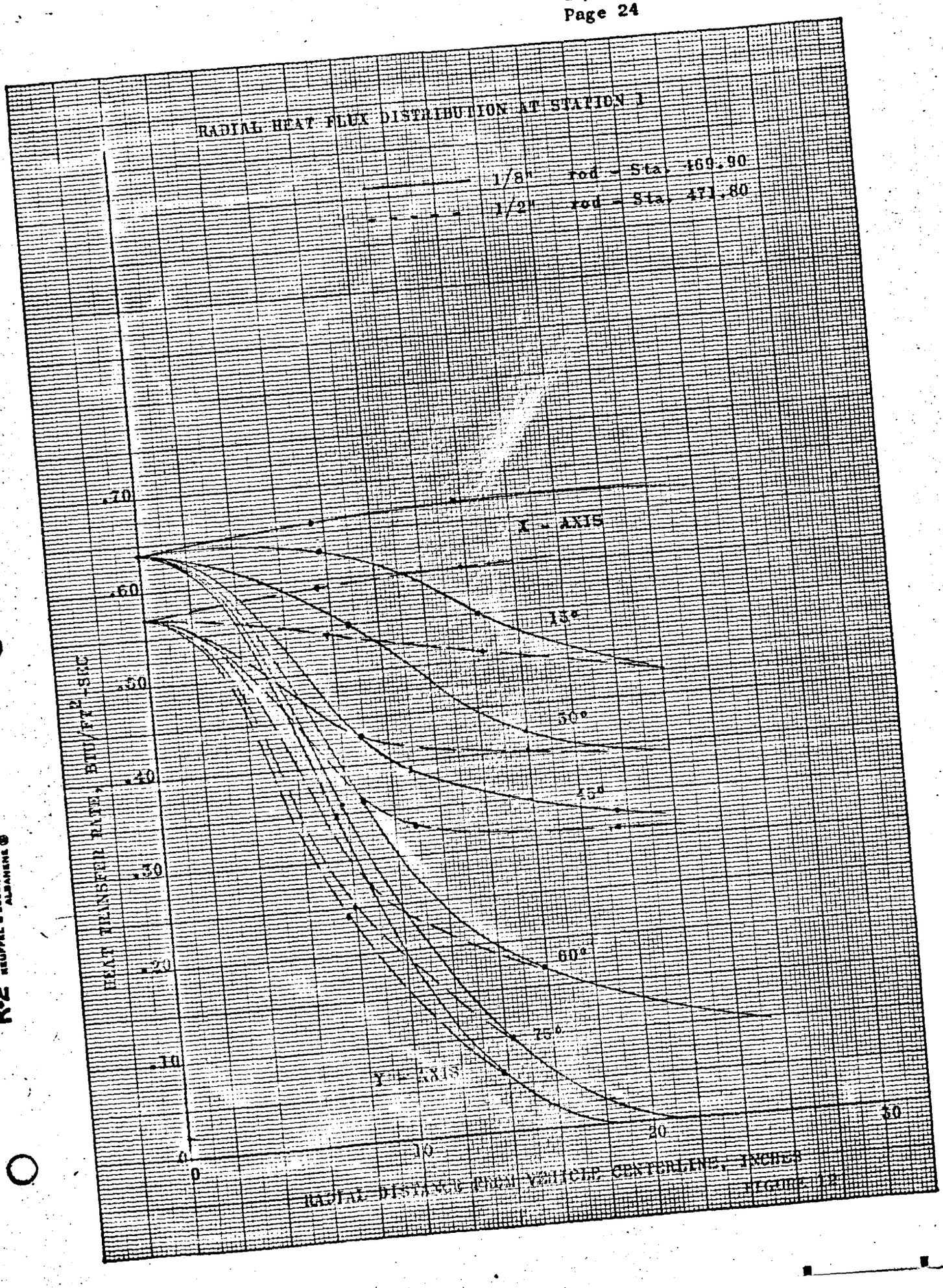

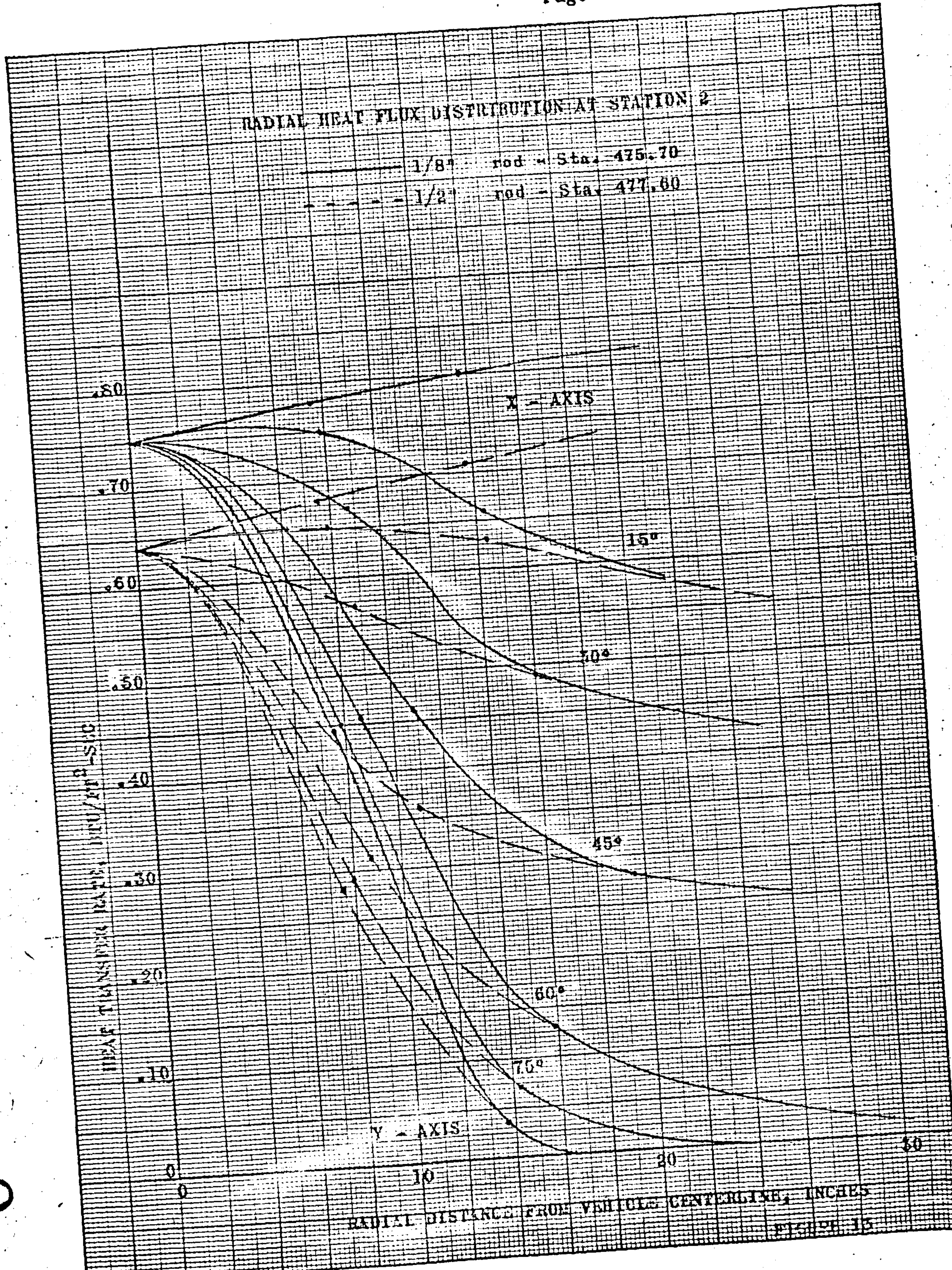

FIGURE 15

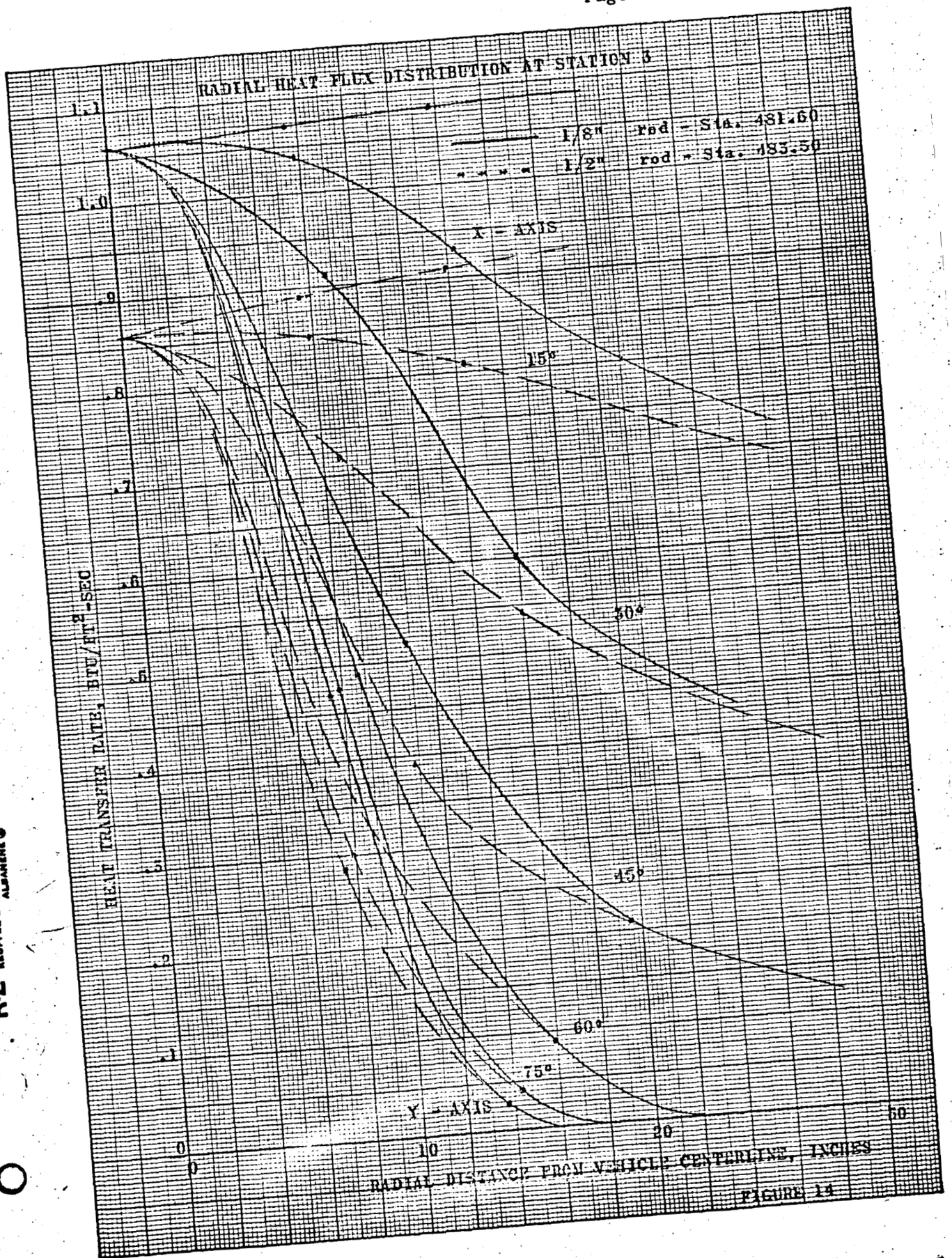
RADIAL HEAT FLUX DISTRIBUTION AT STATION 3
1/8" rod - Sta. 481.60
1/2" rod - Sta. 483.50
X - AXIS
Y - AXIS
15°
30°
45°
60°
75°
HEAT TRANSFER RATE, BTU/FT²-SEC
RADIAL DISTANCE FROM VEHICLE CENTERLINE, INCHES
1.1
1.0
.9
.8
.7
.6
.5
.4
.3
.2
.1
0
10
20
50

FIGURE 14

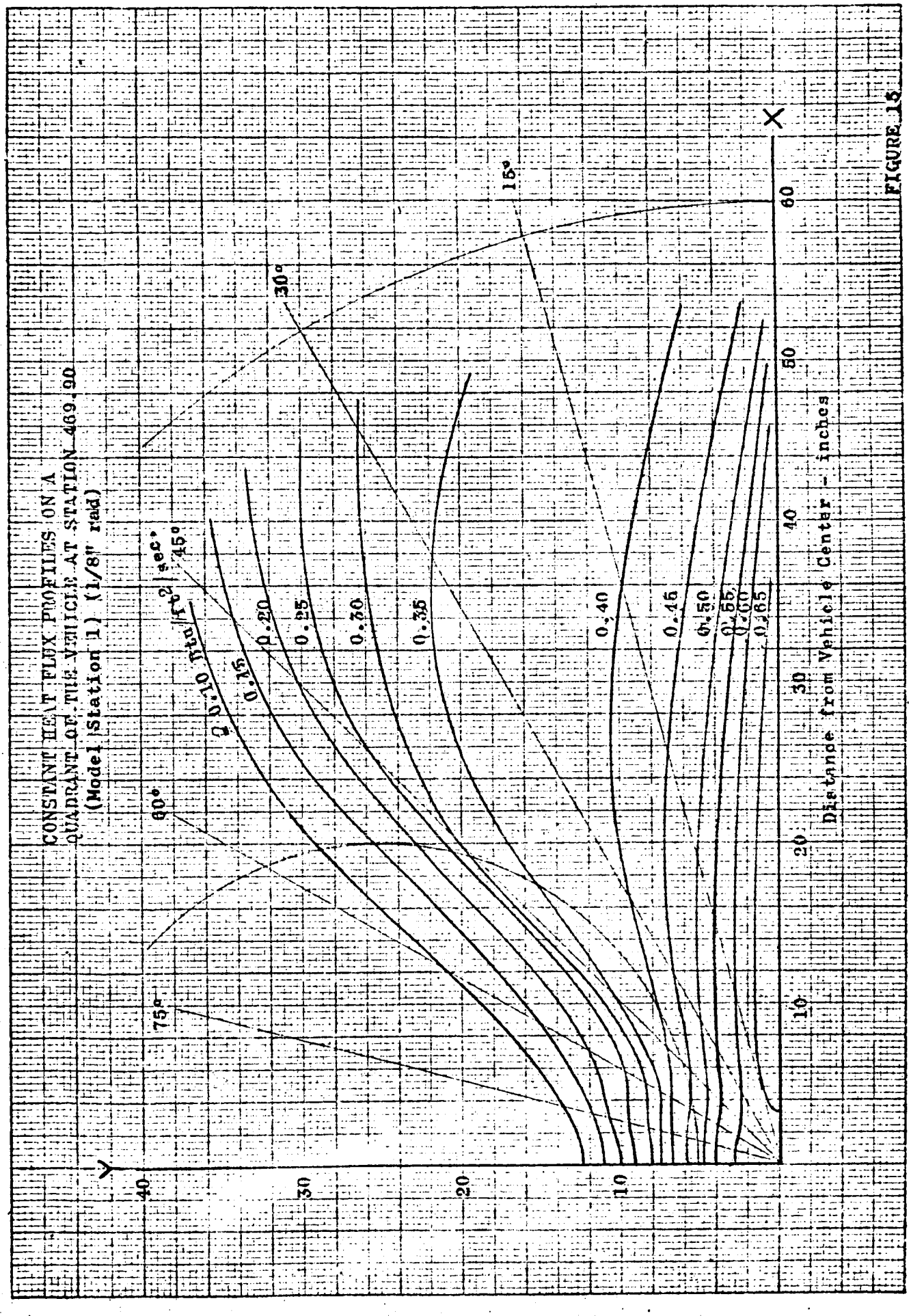
CONSTANT HEAT FLUX PROFILES ON A
QUADRANT OF THE VEHICLE AT STATION 469.90
(Model Station 1) (1/8" rad.)
Q = 0.10 Btu/ft²/sec
0.15
0.20
0.25
0.30
0.35
0.40
0.45
0.50
0.55
0.60
0.65
90°
75°
60°
45°
30°
15°
Y
X
Distance from Vehicle Center - inches
10
20
30
40
50
60

FIGURE 18

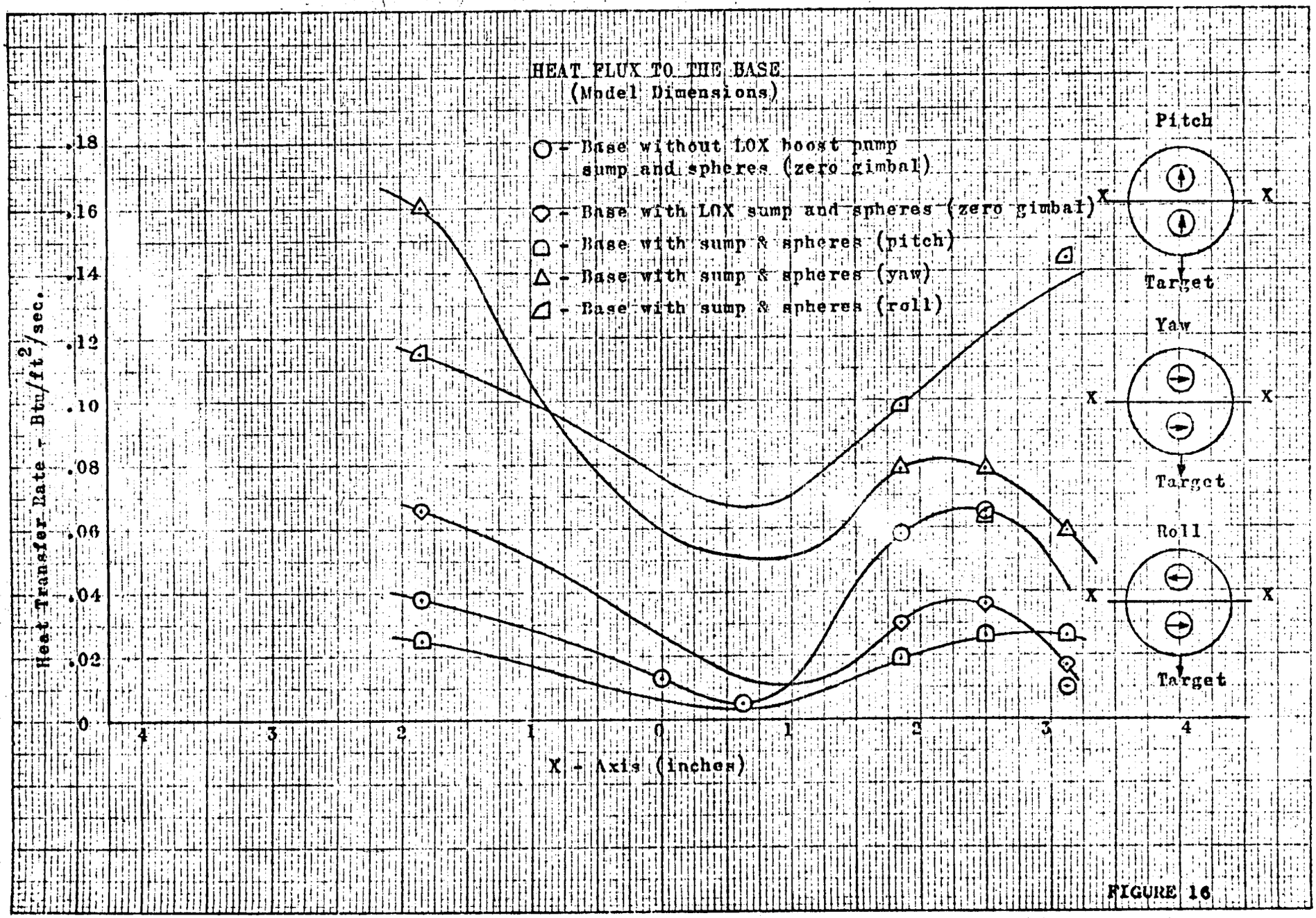
HEAT FLUX TO THE BASE
(Model Dimensions)
○ - Base without LOX boost pump sump and spheres (zero gimbal)
◇ - Base with LOX sump and spheres (zero gimbal)
□ - Base with sump & spheres (pitch)
△ - Base with sump & spheres (yaw)
◺ - Base with sump & spheres (roll)
Heat Transfer Rate - Btu/ft²/sec.
.18
.16
.14
.12
.10
.08
.06
.04
.02
0
4
3
2
1
0
1
2
3
4
X - Axis (inches)
Pitch
X
X
Target
Yaw
X
X
Target
Roll
X
X
Target

FIGURE 16

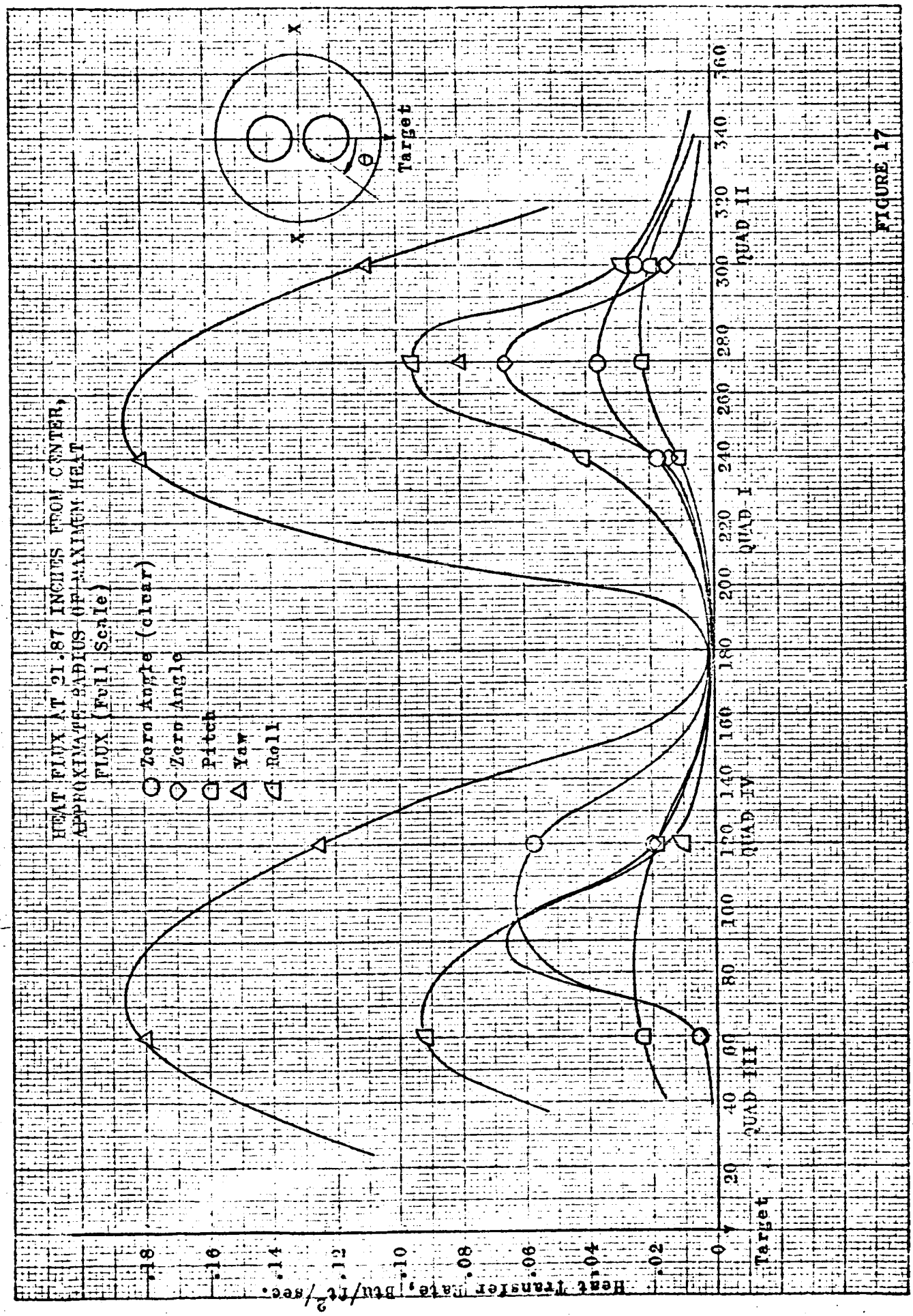
HEAT FLUX AT 21.87 INCHES FROM CENTER,
APPROXIMATE RADIUS OF MAXIMUM HEAT
FLUX (Full Scale)
Zero Angle (clear)
Zero Angle
Pitch
Yaw
Roll
Heat Transfer Rate, Btu/ft²/sec.
.18
.16
.14
.12
.10
.08
.06
.04
.02
0
Target
20
40
60
80
100
120
140
160
180
200
220
240
260
280
300
320
340
360
QUAD III
QUAD IV
QUAD I
QUAD II
Target
θ
x
x

FIGURE 17